Transactions of the Korean Nuclear Society Autumn Meeting
Gyeongju, Korea, October 29-30, 2026

Effect of axial fuel and coolant temperature distribution in the homogenized assembly cross section generation for Boron-Free SMR core

Hyo Yun Lee [1], Sung Hyun Cho [1], Woo Jin Lee [1], Ser Gi Hong [1]*
[1]*Department of Nuclear Engineering, Hanyang University, 222 Wangsimni-ro, Seongdong-gu, Seoul 04763, Korea*
**Corresponding author: hongsergi@hanyang.ac.kr*

Keywords : MASTER, axial temperature distribution, boron-free core, critical rod search, power peaking factor

1. Introduction

The boron-free SMR (Small Modular Reactor) core such as i-SMR uses the control rods as a main reactivity control mechanism in baseload and load-follow operations [1]. This kind of control rod movement can result in the distortion of axial power distribution, leading to the distortion in the axial coolant and fuel temperature distribution. However, the conventional two-step method employs a simple approach for treating temperature effects. In this approach, the depletion calculation in the lattice calculation is performed only at a given set of reference fuel and coolant temperatures. The temperature dependence of the homogenized cross sections is then accounted for through branch calculations at the given burnup points [2]. Nevertheless, the local fuel and coolant temperatures in the core can deviate considerably from the reference temperatures used in the lattice depletion calculation. Although the temperature dependence of the HGCs can be represented through branch calculations, these branch calculations are based on depletion calculations performed at a single set of reference fuel and coolant temperatures. Consequently, the axial variations in fuel and coolant temperatures experienced during depletion are not explicitly reflected in the HGC generation. Therefore, HGCs generated using the conventional reference-temperature depletion treatment may not fully represent the burnup- and temperature-dependent neutronic characteristics of individual axial regions in the actual core.

The objective of this study is to quantify the changes in core calculation results caused by accounting for axial fuel and coolant temperature conditions in the HGC generation. For this purpose, two HGC treatments are compared for the same core configuration and fuel assembly specifications: a Reference treatment using HGCs generated at a single representative temperature condition and an axially temperature-dependent treatment using HGCs generated with representative temperatures for individual axial nodes. A PWR-based SMR core using LEU+ fuels and UN-GdN burnable poison rods [3] is considered. Soluble boron-free depletion calculations are performed with criticality maintained by adjusting the control rod positions, and the resulting changes in the critical rod position and power distribution parameters are evaluated.

2. Computer Codes and Core Design

2.1 Computer Codes

For the neutronic analysis, the two-step procedure with DeCART2D v1.1 [4] and MASTER v4.0 [5], both developed by KAERI, is employed. DeCART2D generates assembly-wise homogenized group constants based on ENDF/B-VII.1, while MASTER performs three-dimensional core nodal diffusion calculations with the Source Expansion Nodal Method (SENM), supporting both steady-state and transient calculation.

In this study, different sets of HGCs were generated by DeCART2D according to the prescribed lattice temperature conditions, and their effects were evaluated through subsequent MASTER core calculations.

2.2 LEU+ fueled SMR core

A small PWR-based SMR core was designed using LEU+ fuels and UN-GdN burnable absorber rods. The core has 180 MW_{th} rated power and is loaded with 37 fuel assemblies. The core is comprised of five types of fuel assemblies, and they have different uranium enrichments, different numbers of burnable absorber (BA) rods, and different GdN contents in UN-GdN BA rods. Their design characteristics are summarized in Table I. UN-GdN BA rods were introduced to effectively control excess reactivity and to utilize its high thermal property [3]. Fig. 1 compares the core loading patterns for cycles 1, 2, and 3. Fig. 2 shows the arrangement of the control rods. There are three regulating banks (R1~R3) and three shutdown banks (S1~S3). Fig. 3 shows the control rod insertion strategy considered in this work.

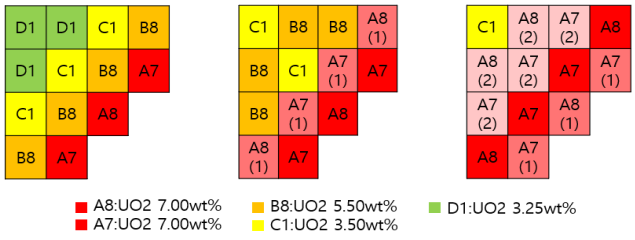


Fig. 1. Core loading patterns used for Cycle 1, Cycle 2, and Cycle 3.

Table I. Design specifications of fuel assemblies

Fuel assembly	GdN wt. %	Number of BA rods
A8	4.3	32
A7	5.3	32
B8	8	24
C1	7.2	24
D1	7.5	24

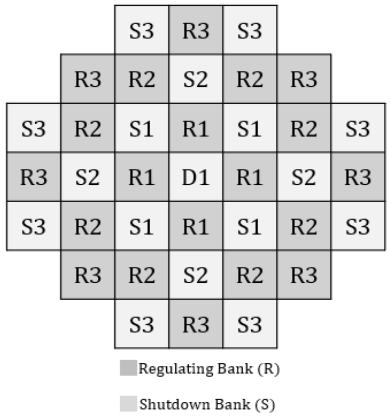


Fig. 2. Arrangement of control rods

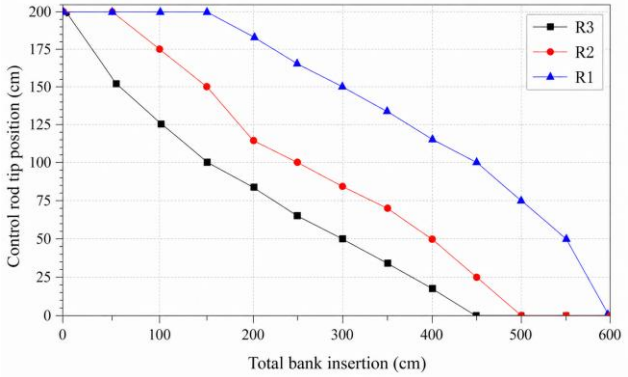


Fig. 3. Regulating bank insertion strategy

2.3 Axial temperature treatment

Two HGC generation treatments were considered to evaluate the effect of axial fuel and coolant temperature conditions on the core calculation results. In the subsequent MASTER calculations, the core configuration, fuel loading pattern, fuel assembly specifications, depletion steps, and control rod search procedure were kept identical between the two treatments. The difference between the two calculations was the HGC set assigned to the axial nodes, which was generated using different lattice depletion temperature conditions.

For the Reference case representing conventional treatment, the DeCART2D lattice depletion calculations were performed at the single representative fuel and coolant temperatures of 626.85 °C and 306.85 °C, respectively, and the resulting HGCs were used in the MASTER core calculations. In this work, to consider the axial temperature distribution in the lattice calculation, the axial fuel and coolant temperatures were taken from the core calculation results of the Cycle 1 Reference MASTER calculation and used in the DeCART2D lattice calculations. Fig. 4 shows an example of the axial temperature conditions used for HGC generation in the Reference and axially temperature-dependent treatments.

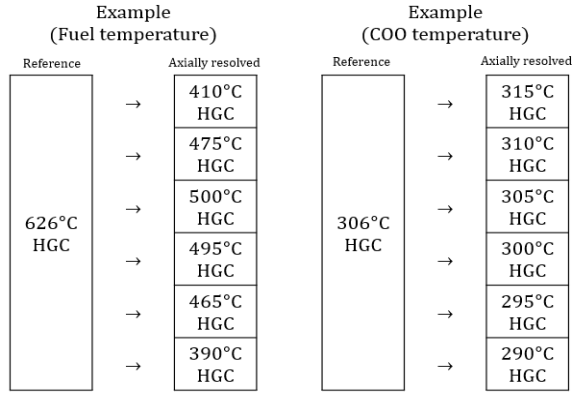


Fig. 4. Schematic example of the Reference and axially temperature-dependent HGC generation treatments.

Both the Reference and Axially temperature-dependent cases were analyzed using soluble boron-free depletion calculations, with the control rod positions adjusted through a rod search to maintain criticality throughout the depletion calculation. For the Axially temperature-dependent calculation, fuel and coolant temperature profiles, shown in Fig. 5, were extracted from the MASTER results for the first cycle. The profiles were depletion-averaged and represented using 20 axial nodes, each 10 cm in height, along the 200-cm active core height. The same axial temperature profiles obtained from the first-cycle calculation were also used to generate the HGC files for the second and third cycles. For each axial node, a separate DeCART2D lattice depletion calculation was performed using the corresponding representative fuel and coolant temperatures. The resulting HGCs were then assigned to the corresponding axial nodes in the subsequent MASTER calculation. Accordingly, the comparison was designed to evaluate the overall effect of the HGC generation treatment in which the axial temperature conditions are incorporated into the lattice depletion and HGC generation.

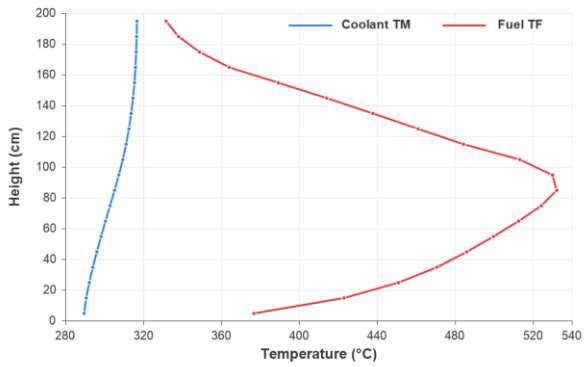


Fig. 5. Depletion-averaged axial fuel and coolant temperature distributions obtained from the Reference MASTER calculation for Cycle 1.

The node-wise temperature conditions derived from the Cycle 1 Reference calculation were also used for Cycles 2 and 3. Therefore, the same set of axially temperature-dependent HGCs based on the Cycle 1 temperature distribution was applied throughout the three-cycle calculation.

3. Results and Discussion

3.1 Effect on boron-free depletion parameters

Figures 6–9 compare the critical regulating-bank position, axial offset (AO), three-dimensional power peaking factor (F_q), and radial power peaking factor (F_r) histories for Cycle 1 between the Reference case and Axially temperature-dependent case. The results show similar overall trends between the reference and Axially temperature-dependent case, but systematic differences remain throughout the depletion history because the Axially temperature-dependent treatment changes the local cross sections and hence the critical positions of the control rods.

For Cycle 1, the differences in the critical regulating-bank position, F_q, and AO between the two calculations reached their maximum values at the same depletion point. In particular, the maximum absolute differences in the critical regulating-bank position, F_q, and AO reached 3.375 cm, 0.168, and 0.031, respectively. In contrast, the difference in F_r initially decreased but began to increase again from the middle of the cycle, reaching its maximum value of 0.009 at the end of the cycle.

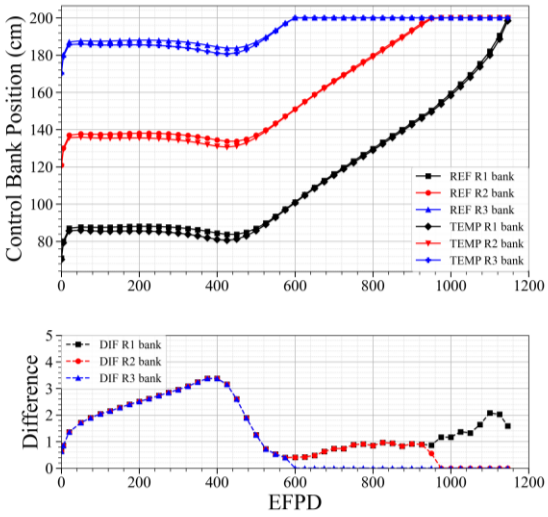


Fig. 1. Critical rod position of regulating bank for Cycle 1.

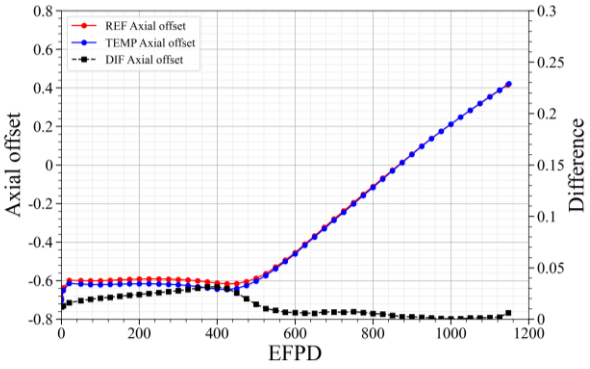


Fig. 2. Axial offset as depletion for Cycle 1.

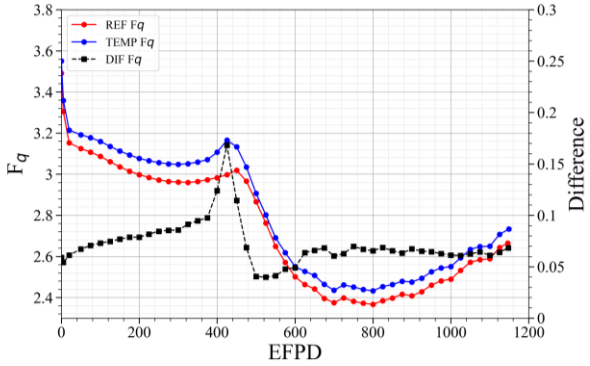


Fig. 3. F_q as depletion for Cycle 1.

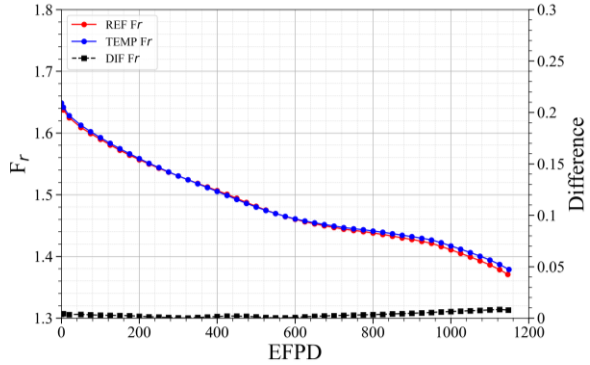


Fig. 4. F_r as depletion for Cycle 1.

Because the temperature distribution was considered only in the axial direction and radial temperature variations were not considered, relatively large differences were observed in F_q and AO, whereas the difference in F_r remained relatively small.

Table II summarizes the cycle-averaged differences and maximum absolute differences in critical rod position and power distribution between the Axially temperature-dependent and Reference calculations. The cycle-averaged difference is calculated as the axially temperature-dependent result minus the corresponding reference result.

Table II. Cycle averaged and maximum absolute differences in critical rod position and power distribution

critical rod position				
Cycle	Ref_avg	Temp_avg	Avg_diff	Max_diff
CY01	167.826	166.693	-1.133	3.375
CY02	151.046	150.175	-0.871	5.894
CY03	158.702	158.264	-0.438	4.596

AO				
Cycle	Ref_avg	Temp_avg	Avg_diff	Max_diff
CY01	-0.309	-0.320	-0.013	0.031
CY02	-0.095	-0.108	-0.013	0.026
CY03	-0.089	-0.100	-0.011	0.030

F_q				
Cycle	Ref_avg	Temp_avg	Avg_diff	Max_diff
CY01	2.722	2.794	+0.072	0.168
CY02	2.617	2.665	+0.048	0.173
CY03	2.339	2.388	+0.049	0.121

F_r				
Cycle	Ref_avg	Temp_avg	Avg_diff	Max_diff
CY01	1.483	1.485	+0.003	0.009
CY02	1.462	1.464	+0.002	0.010
CY03	1.463	1.478	+0.015	0.038

For Cycles 2 and 3, the critical regulating-bank positions show smaller cycle-average differences between the Reference and Axially temperature-dependent cases than in Cycle 1. However, the rod-position differences increase toward the end of the cycles, resulting in larger maximum differences than those observed in Cycle 1. The differences in the power peaking factors are generally smaller than or comparable to those in Cycle 1, although the maximum F_q difference remains greater than 0.1. Non-negligible differences also remain in AO, while the difference in Fr remained relatively small throughout the subsequent cycles.

Overall, the depletion calculations with critical rod searches shows that the Axially temperature-dependent treatment produces non-negligible differences in both rod-insertion history and peaking factors. The effect is not a simple uniform reactivity bias because local cross section changes modify the spatial flux and power distributions.

4. Conclusions

In this work, the effect of accounting for axial fuel and coolant temperature conditions in HGC generation was investigated by comparing the fixed reference-temperature and axially temperature-dependent HGC treatments in MASTER soluble-boron-free control rod depletion calculations.

Across Cycles 1–3, both HGC treatments showed similar rod insertion trends but noticeable differences in the critical regulating-bank position, AO, and power peaking factors. The maximum absolute regulating bank position and F_q differences reached 5.894 cm and 0.173, respectively. These results show that the use of HGCs generated at a single reference-temperature condition, rather than HGCs generated with representative axial temperature conditions, can lead to noticeable differences in the rod insertion history and local power distribution of a soluble boron-free core. Therefore, the temperature conditions used in HGC generation can produce noticeable differences in the predicted control rod positions and local power distributions in soluble boron-free depletion calculations.

In future work, the axial temperature distribution will be determined iteratively by coupling the lattice and core calculations, instead of the one-pass HGC update based on the Reference-case temperature distribution used in this work. In addition, more realistic control bank configurations will be considered, since the bank pattern in this work was selected for the sensitivity comparison rather than for the optimized core control.

5. Acknowledgment

This work was supported by the Korea Institute of Energy Technology Evaluation and Planning (KETEP) and the Ministry of Climate, Energy & Environment (MCEE) of the Republic of Korea. (No. RS-2024-00398867).

REFERENCES

[1] H. O. Kang, B. J. Lee, and S. G. Lim, “Light Water SMR Development Status in Korea,” Nuclear Engineering and Design, Vol. 419, 112966, 2024.

[2] I. Bilodid and S. Mittag, “Use of the Local Pu-239 Concentration as an Indicator of Burnup Spectral History in DYN3D,” Annals of Nuclear Energy, Vol. 37, No. 9, pp. 1208-1213, 2010.

[3] S. T. Oh and S. G. Hong, “Effectiveness of UN-GdN Burnable Absorber for 180MWt SMR Core Loaded with LEU+ Fuels,” Transactions of the Korean Nuclear Society Spring Meeting, Jeju, Korea, May 7-8, 2026.

[4] J. Y. Cho, et al., “DeCART2D v1.1 User’s Manual,” KAERI/UM-40/2016, 2016.

[5] J. Y. Cho, et al., “MASTER v4.0 User’s Manual,” KAERI/UM-41/2016, 2016.